

Assessment of masonry arch bridges retrofitted by sprayed concrete under in-plane cyclic loading

Mahdi Yazdani^{*1} and Mehrdad Zirakbash^{2a}

¹Department of Civil Engineering, Faculty of Engineering, Arak University, Arak, Iran

²Faculty of Civil Engineering and Transportation, University of Isfahan, Isfahan, Iran

(Received December 26, 2023, Revised March 8, 2024, Accepted March 20, 2024)

Abstract. Masonry arch bridges as a vital infrastructure were not designed for seismic loads. Given that masonry arch bridges are made up of various components, their contribution under the seismic actions can be very undetermined and each of these structural components can play a different role in energy dissipation. Iran is known as a high-risk area in terms of seismic excitations and according to the seismic hazard zoning classification of Iran, most of these railway infrastructures are placed in the high and very high seismicity zones or constructed near the major faults. Besides, these ageing structures are deteriorated and thus in recent years, some of these bridges using various retrofitting approaches, including sprayed concrete technique are strengthened. Therefore, investigating the behavior of these restored structures with new characteristics is very significant. The aim of this study is to investigate the cyclic in-plane performance of masonry arch bridges retrofitted by sprayed concrete technique through the finite element simulation. So, by considering the fill-arch interaction, the nonlinear behavior of a bridge has been investigated. Finally, by extracting the hysteresis and enveloping curves of the retrofitted and non-retrofitted bridge, the effect of strengthening on energy absorption and degradation of material has been investigated.

Keywords: cyclic loading; energy absorption; finite element modeling; masonry arch bridges; retrofitting; sprayed concrete

1. Introduction

Masonry arch bridges as a vital infrastructure are available in large numbers in the world's rail and road transportation networks. There are approximately one million masonry arch bridges in road and railway networks worldwide, with the majority located in Europe. In Iran, due to the 90-year-old lifetime of the railway network, there are numerous masonry arch bridges. Presently, about 3,500 masonry arch bridges serve as rail infrastructure. Most of these aging bridges are efficiently handling loads significantly greater than their design live loads. However, insufficient knowledge regarding their seismic behavior has become a serious concern. Since these monument structures were not designed for seismic loads, their seismic behavior strongly has been of great interest in recent years (Gönen and Soyöz 2022, 2021, Pantò *et al.* 2022, Mahmoudi Moazam *et al.* 2018). Given that masonry arch bridges are made up of various components including arch, spandrel wall, abutment,

*Corresponding author, Associate Professor, E-mail: m-yazdani@araku.ac.ir

^aM.sc. Student, E-mail: zirakbashmehrdad@gmail.com

pier, wing wall and backfill, their contribution under the influence of seismic loads can be very complex and each of these structural components in term of structural integrity can play a different role in energy dissipation. Furthermore, masonry arch bridges are made of various materials such as brick, stone, and unreinforced concrete, posing challenges in investigating their behavior. On the other hand, due to limitations of cost and time aspects, replacing these magnificent historical structures is not practicable. Therefore, in term of infrastructure management, the preservation, maintenance, and continuous monitoring, followed by restoring, repairing, and strengthening, hold great importance. Despite various empirical, analytical, and numerical methods to calculate the load-carrying capacity of masonry arch bridges under vertical (gravity) loads (Panian and Yazdani 2020, Sarhosis *et al.* 2016, Wang and Melbourne 2010, Yazdani 2021, Yazdani and Habibi 2023), knowledge about their seismic capacity (lateral loads) is limited (Marefat *et al.* 2019). Various methods exist for seismic analysis of structures, including linear static analysis, linear dynamic analysis, nonlinear static analysis, and nonlinear dynamic analysis. Considering the limitations of linear static analysis and the development of nonlinear concepts on one side, and the developing discussion on performance-based design methods on the other, significant efforts have been made in recent years to design and evaluate structures based on displacement and direct use of nonlinear analysis to assess structure performance against different earthquake intensities. Additionally, to address economic issues and optimize the use of energy absorption and dissipation properties in the plastic range, members are allowed to undergo non-linear behavior during severe earthquakes and engage in energy absorption through plastic deformations under earthquake reciprocating loads. Consequently, the structure's behavior against strong earthquake excitations is nonlinear. So, besides strength and stiffness, ductility is of crucial importance in the design parameters (Zampieri *et al.* 2015).

Iran is known as the fifth most earthquake-prone country, so Iran is a high-risk area in terms of seismic action. The previous studies indicated that the masonry arch bridges are vulnerable under seismic actions in which the highest confidence level is obtained under lower intensities but the confidence level of them decreases when the level of earthquake intensity increases and it seems that retrofitting of them is necessary (Homaei and Yazdani 2020). There are abundant methods to retrofitting the masonry arch bridges. For example, the IRS 70778-3 standard (Recommendations for inspection, assessment and maintenance of masonry arch bridges) proposed: (1) implanting transverse tie bars in arch barrel, (2) sprayed concrete, (3) adding internal spandrel walls, (4) adding concrete saddle, (5) using carbon fiber reinforced plastic strips, (6) adding steel arches under the arch barrel, (7) adding concrete slab over an arch, (8) fill injection systems and (9) using geocomposite raft. Also, recently Wang *et al.* (2022) presented a suitable analytical approach to retrofit of masonry arch bridges. So, they implemented four strengthening configurations including intrados, extrados, U-hoop and box-hoop to reinforce masonry arch bridges with ultrahigh-performance concrete materials (Wang *et al.* 2022). Drosopoulos *et al.* (2007) used FRP for retrofitting masonry arch bridges in which three types of strengthening were applied to the arch: (1) FRP was attached to the whole length of the extrados, (2) FRP was attached to the whole length of the intrados and (3) FRP was attached to the extrados and the intrados of the arch simultaneously. They concluded interior reinforcement has a higher ultimate load in comparison with exterior reinforcement (Drosopoulos *et al.* 2007). D'Ambrisi *et al.* (2013) used PBO-FRCM materials and proposed a new retrofitting technique for railway masonry arch bridges. They showed this technique increases the capacity of these infrastructures up to 40% under service loads (D'Ambrisi *et al.* 2013). Simoncello *et al.* (2020) using an experimental study on masonry arch bridges which strengthened with a layer of FRP applied at the intrados. The results of their study indicated that the ultimate capacity of

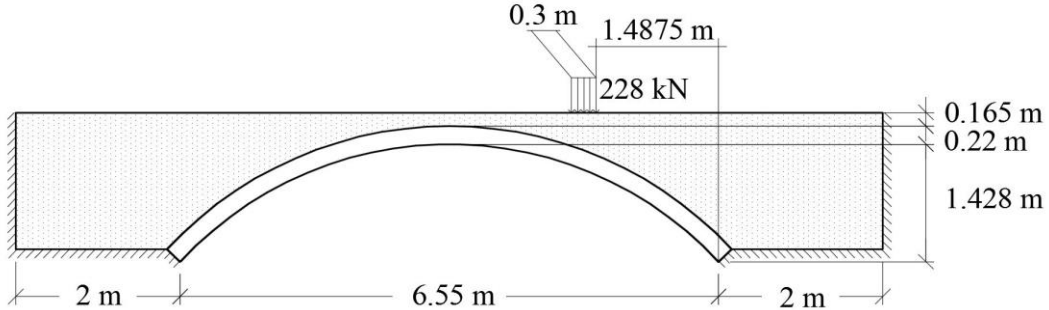


Fig. 1 Geometrical properties of Prestwood bridge as a benchmark (Drosopoulos *et al.* 2007)

bridge is significantly increased (Simoncello *et al.* 2020).

Although extensive research has been conducted on the seismic behavior of masonry arch bridges, the hysteresis behavior resulting from lateral cyclic loads has received less attention. Therefore, the purpose of this study is to investigate the in-plane cyclic behavior of a retrofitted masonry arch bridge using sprayed concrete technique to extract the hysteresis curve of the bridge before and after retrofitting to assess the performance of the masonry arch bridges. So, in the second section the numerical model has been constructed and after validation of finite element model under vertical loading, in the next section the numerical models have been simulated under seismic actions by nonlinear static method. After that in the fourth section the hysteresis analysis has been taken into account and finally in the fifth section the conclusions have been presented.

2. Numerical model

In this study, a benchmark example was utilized to construct the numerical model, as depicted in Fig. 1 (Drosopoulos *et al.* 2007). For this purpose, a finite element model of the Prestwood Bridge was created in the ANSYS finite element package. Considering the predominantly two-dimensional behavior of masonry arch bridges, plane strain analysis was chosen (Azimi and Yazdani 2022). Thus, high-order 8-node elements were used to generate the meshing of finite element model.

The effect of fill-arch interaction has also been considered. To achieve this, two sets of interfaces were simulated. The first simulation contains of a direct connection between the backfill and arch nodal elements and in the second simulation, according to the Coulomb friction model which is demonstrated in Fig. 2, an interface was attached between the arch and the backfill surface to account considering sliding. The sliding resistance of the arch surface on the backfill is computed as (Homaei and Yazdani 2020)

$$T_{ult} = \mu W_{tot} + A_f C \quad (1)$$

where W_{tot} is the total vertical force on the surface of the backfill, C is the backfill contact cohesion on the arch area (A_f), and μ is the friction coefficient between the arch and backfill surface. In the basic Coulomb friction model, two contacting faces can transfer shear stresses up to a definite magnitude across the interface before they initiate sliding relative to each other. This state is recognized as sticking property. The Coulomb friction model defines equivalent shear stress at which

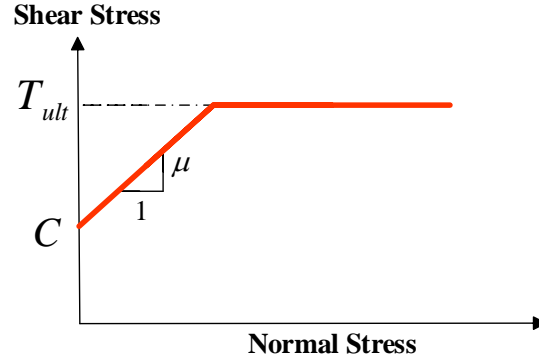


Fig. 2 The classical Coulomb friction model for simulation sliding on fill-arch interaction

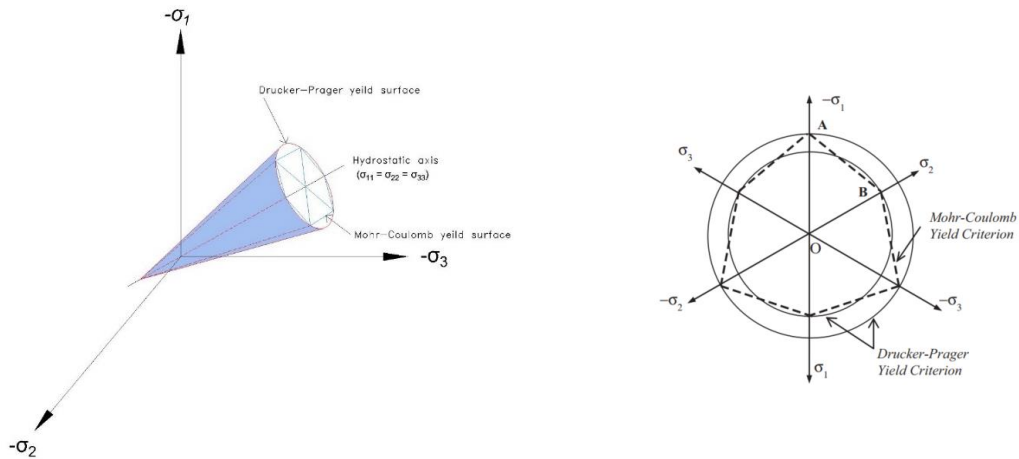


Fig. 3 The Drucker-Prager and Mohr-Coulomb yield criteria

sliding on the surface starts as a fraction of the contact pressure ($\mu W_{tot} + A_f C$). After the shear stress is exceeded, the two faces will slide relative to each other. This state is identified as sliding feature. The sticking and sliding calculations define when a point transitions from sticking to sliding or vice versa.

Afterward in this study, an elastoplastic model with the Drucker-Prager yield criterion was used for materials. Based on the Fig. 3, this criterion was developed by soothing the surface of the Von Mises yield and Mohr-Coulomb criteria.

It contains the effect of hydrostatic pressure on the shear resistance of materials. The general form of the Drucker-Prager yield surface is expressed as (Chen, 2007)

$$f(I_1, J_2) = \sqrt{J_2} - \alpha I_1 - k = 0 \quad (2)$$

In Eq. (2), I_1 and J_2 are positive constants. Explicitly, I_1 is the first invariable of Cauchy stresses and J_2 is the second invariable of the deviatorial Cauchy stresses. Also, α is material constant and k

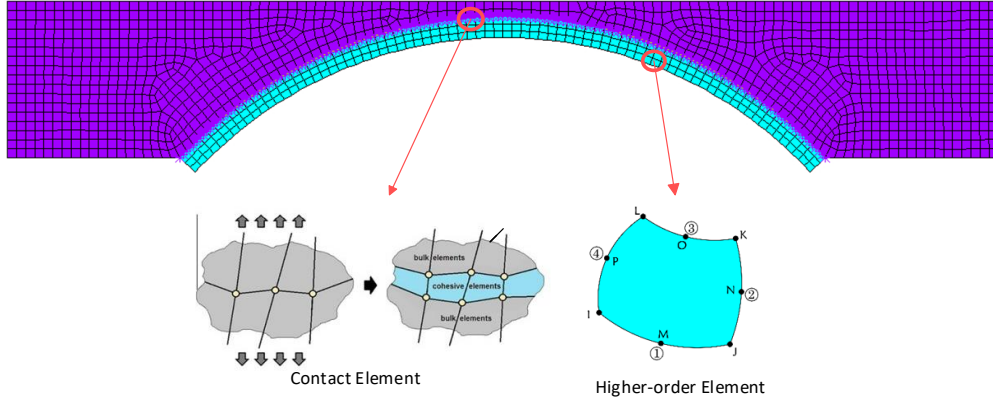


Fig. 4 The initial finite element model of considered benchmark bridge

Table 1 Mechanical properties of materials

Materials	Density (kg/m ³)	Modulus of elasticity (GPa)	Poisson ratio	Cohesion coefficient (KPa)	Friction angle (Degree)	Dilatancy angle
arch	2000	15	0.3	1000	45	9.2
backfill	2000	0.3	0.3	100	37	5

is the material yield parameter. In such a model, the Drucker-Prager parameters are expressed as (Chen 2007)

$$\alpha = \frac{2 \sin \phi}{\sqrt{3}(3 \pm \sin \phi)} \tag{3}$$

$$k = \frac{6c \cos \phi}{\sqrt{3}(3 \pm \sin \phi)} \tag{4}$$

where ϕ and c are the friction angle and cohesion coefficient, respectively. Therefore, the input parameters of Prestwood bridge based on the Drucker-Prager criterion were directly obtained, as shown in Table 1.

Consequently, the initial numerical model of the bridge is demonstrated in Fig. 4. It is worth to mention the numerical model consisted of 1,343 eight-node elements and 235 contact elements, resulting in a total of 4,447 nodes for the entire structure.

2.1 Numerical analysis of the bridge before retrofitting

In the next step, to validate the numerical model, in accordance with the conducted experiment, the bridge was loaded until the failure mechanism is formed. In this step the model calibration parameters are changed in model updating procedure until the experimental and the numerical results converge together and the value of friction coefficient is selected as calibration criteria.

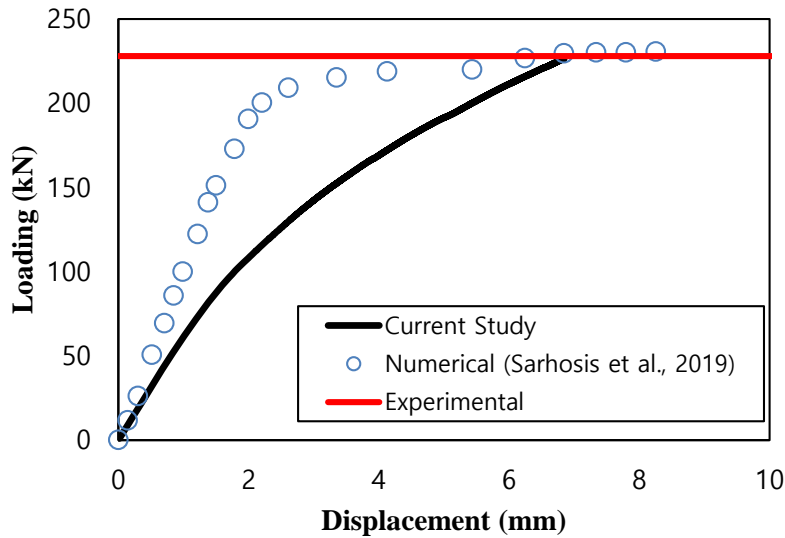


Fig. 5 The load-displacement response of considered bridge under vertical load (Sarhosis *et al.* 2019)

Finally, in this study after model updating process of numerical model, contact elements with the value of $\mu = 0.2$ between the arch and the backfill were employed to account the fill-arch interaction.

In the nonlinear static analysis, element matrices are calculated by the Gaussian numerical integration. Also, the nonlinear static analysis is solved by the Newton–Raphson algorithm with a load increment of 0.1 kN. Lastly, by defining the displacement and force as convergence criterion, the capacity of the Prestwood bridge is computed. The failure load value determined in the experiment, which was 228 kN, was chosen as the calibration criterion. As observed in Fig. 5, the final capacity of numerical model is converged to 226.7 kN, with an error of only 0.5%, indicating a very appropriate level of accuracy. Afterward, due to the dynamic nature of earthquake excitations, modal analysis was utilized for the second step of validation. The calculated frequency for the first mode is 22.292 Hz, showing a difference of less than 0.4% compared to the value 22.372 Hz which is reported in (Mahmoudi Moazam *et al.* 2017).

2.2 Numerical model of the bridge after retrofitting

Recently, in Iran some of masonry arch bridges using sprayed concrete technique have been retrofitted as depicted in Fig. 6. So, in this subsection the numerical study of retrofitted masonry arch bridges which strengthened by sprayed concrete method is taken into account.

After validating the numerical model, in the next step, a 10 cm concrete layer was modeled under the intrados of the arch (see Fig. 7). To consider the interaction between the arch and the concrete layer, contact elements with a friction coefficient of 0.9 were utilized. An elastoplastic model with the Drucker-Prager yield criterion was also employed to model the concrete. Considering the uniaxial yield compression (σ_c) and tension (σ_t) stresses, Eq. (2) may be expressed as following (Chen 2007)



Fig. 6 A typical retrofitted masonry arch bridge by sprayed concrete technique in Iranian railway network

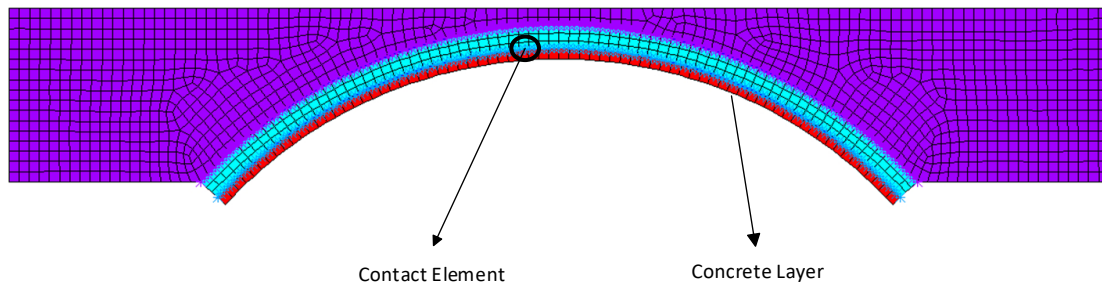


Fig. 7 The numerical model of bridge that retrofitted by sprayed concrete

$$\frac{1}{\sqrt{3}} \sigma_t = k + \alpha \sigma_t \quad (5)$$

$$\frac{1}{\sqrt{3}} \sigma_c = k - \alpha \sigma_c \quad (6)$$

So, the α and k parameters are

$$\alpha = \frac{m-1}{\sqrt{3}(m+1)} \quad (7)$$

$$k = \frac{\sigma_c}{\sqrt{3}(m+1)} \quad (8)$$

where m denotes the relative portion of compressive strength of the concrete material to its tensile strength

$$m = \frac{\sigma_c}{\sigma_t} \quad (9)$$

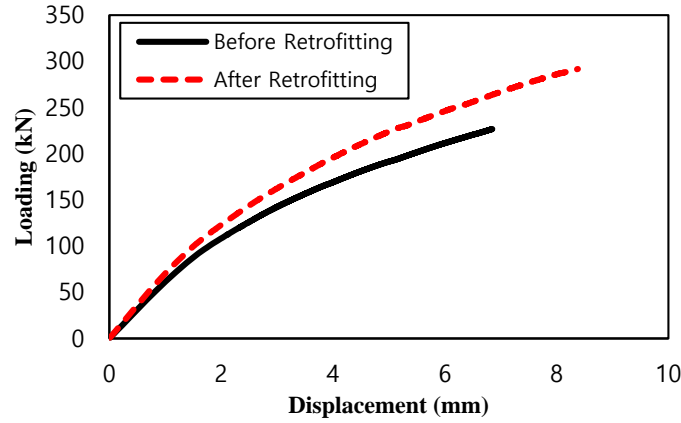


Fig. 8 The comparison of vertical load-displacement response (live load capacity) of Prestwood bridge before and after the retrofitting

Table 2 Mechanical properties of concrete material used for retrofitting of considered bridge

Compressive strength (MPa)	Tensile strength (MPa)	Density (kg/m ³)	Modulus of elasticity (GPa)	Poisson ratio	α	k	Cohesion coefficient (KPa)	Friction angle (ϕ)	Dilatancy angle (ψ)
25	2.8	2400	28.5	0.2	0.461	1.454	4183	53	53

In Eq. (9), almost $8 \leq m \leq 10$. It is worthwhile to mention, the tensile strength of the concrete was also considered $\sigma_t = 0.56\sqrt{\sigma_c}$ based on ACI 318-11 (ACI, 2008). Based on the concrete's compressive strength of 25 MPa, the input parameters for the Drucker-Prager criterion were directly obtained, as shown in Table 2. It is worth to mention for concrete materials due to associated plastic flow rule, the value of dilatancy angle is considered equal to friction angle; so $\psi = \phi = 53^\circ$.

Following this, the ultimate capacity similar to previous section for the Prestwood bridge before and after retrofitting were obtained, as depicted in Figure 8. The numerical results indicated a load of 291.7 kN, which is an approximate 28% increase the failure load of the bridge under vertical loading, while the deformation of the bridge increased by only 21%. The comparison of the failure mechanism of the bridge before and after failure is demonstrated in Fig. 9. Furthermore, the calculated frequency for the first mode was 22.236 Hz, indicating a slight reduction. The first mode shape of the Prestwood bridge which is extracted based on Block Lancsoz method is illustrated in Fig. 10.

3. Seismic capacity

After validating the numerical model under vertical loading, the nonlinear static analysis is performed to investigate the in-plane seismic behavior of the Prestwood bridge. To obtain the seismic capacity curve, a lateral load proportional to the mass and the first mode shape of the structure was applied laterally to the numerical model. By selecting the crown of the bridge at the keystone as the control point (Yazdani and Jahangiri 2020), the load-displacement curve is derived

as displayed in Fig. 11. As it is clear, the lateral capacity of the retrofitted bridge is 379 kN, representing an approximately 61% increase compared to the lateral capacity of the bridge before retrofitting i.e., 235 kN. This increase is achieved while the deformation of the bridge has increased by 120%. Fig. 12 depicts the failure mechanism of the bridge under lateral actions. As it is shown the failure mechanism deforms due to the separation of the backfill from the arch (unlike vertical loads), underscoring the significance of the fill-arch interaction under lateral loads.

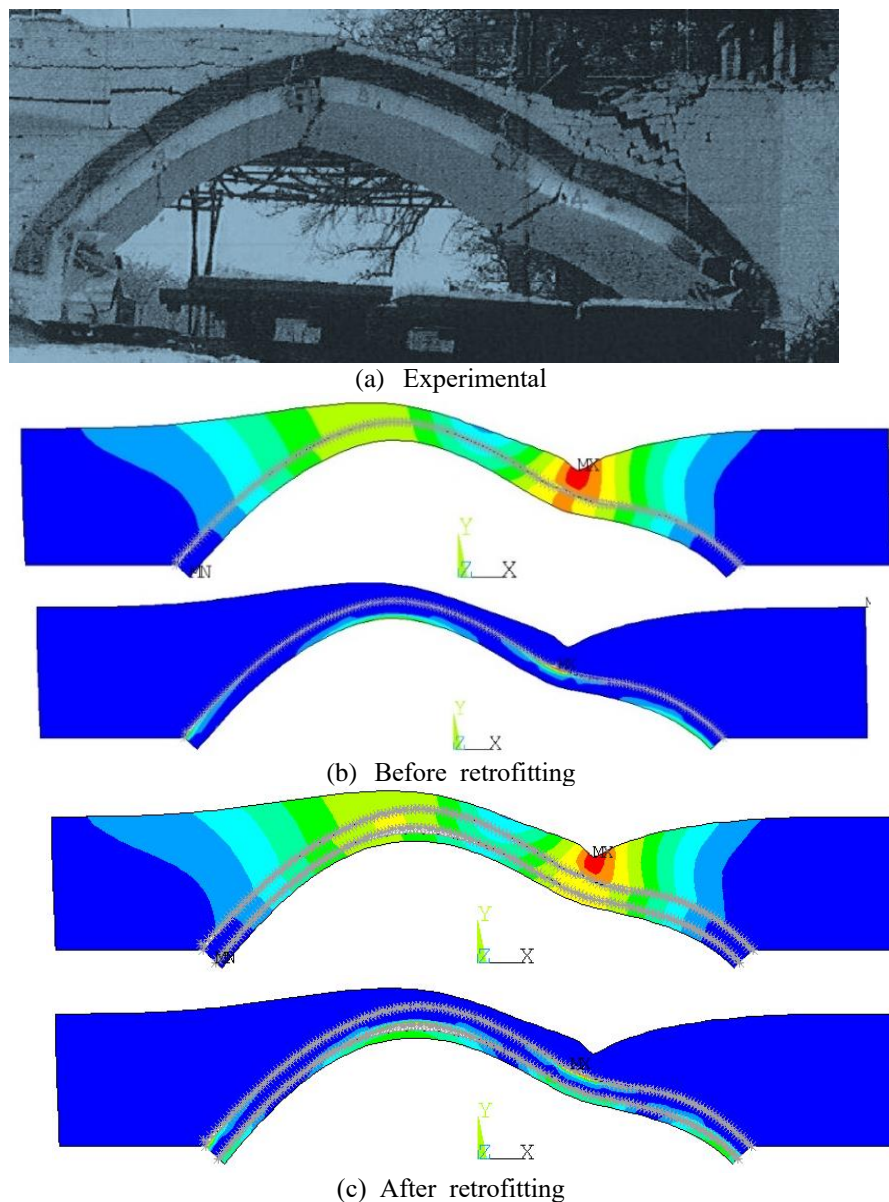


Fig. 9 The four-hinged failure mechanism deformation of Prestwood bridge under vertical loads

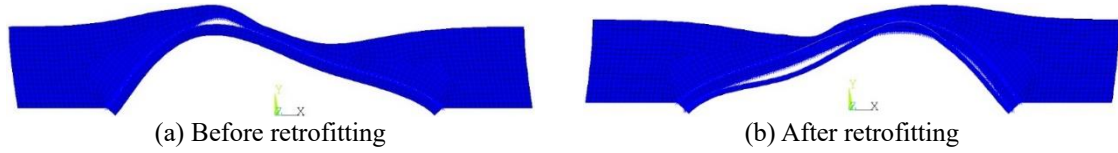


Fig. 10 The first mode shape of Prestwood bridge

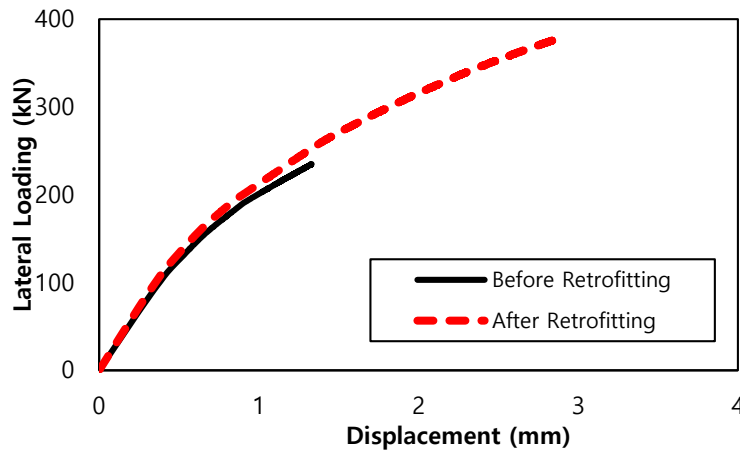


Fig. 11 The comparison of horizontal load-displacement response (in-plane lateral seismic capacity) of Prestwood bridge before and after the retrofitting

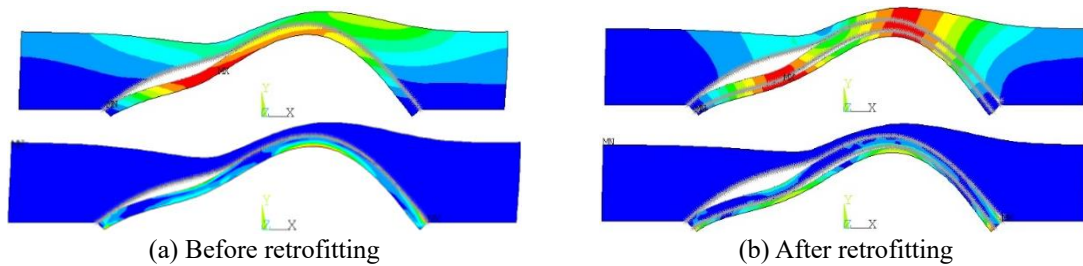


Fig. 12 The failure mechanism deformation of Prestwood bridge under lateral (seismic) loads

4. Hysteresis curve

After obtaining the desired seismic capacity curve, different percentages of it were cyclically applied to the bridge in order to extract the hysteresis curve in a back-and-forth manner. The obtained response is displayed in Fig. 13. The results indicates that the hysteresis curve illustrates cyclic creep or progressive ratcheting behavior under seismic loads.

Afterward to assess the seismic performance of Prestwood bridge the derivation process of bilinear idealized curves of actual loading-displacement responses is discussed. This idealization is found based on four parameters ultimate strength (V_{max}), yield strength (V_u), maximum displacement (d_u) and yield displacement (d_y). The bilinear idealization of capacity curve is gained

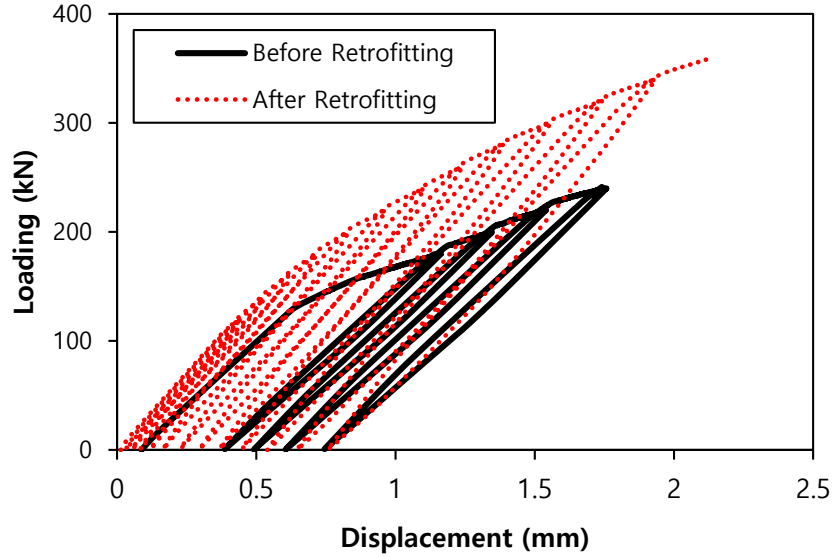


Fig. 13 The hysteresis curve of Prestwood bridge under seismic action

Table 3 The features of bilinear idealized curve for Prestwood bridge

	K_e (kN/mm)	d_y (mm)	d_u (mm)	V_{max} (kN)	μ_d	E_D (kN.mm)
Before retrofitting	232	0.91	1.33	235	1.46	185
After retrofitting	232	1.47	2.90	379	1.98	740
Difference (%)	0	+61	+118	+61	+35	+300

based on equal energy principle which is fulfilled as the ratio of $V_u/V_{max} = 0.9$ that suggested by Magenes and Calvi for masonry structures (Magenes and Calvi, 1997). Estimation of bilinear curves is necessary for interpret the result of lateral capacity curves and consequently helpful for extracting various parameters which among them the effective stiffness (K_e) and ductility factor (μ_d) are used in this paper and calculated by Eqs. (10) to (12), respectively.

$$K_e = \frac{\alpha V_u}{d_\alpha} \quad (10)$$

$$d_y = \frac{V_u}{K_e} \quad (11)$$

$$\mu_d = \frac{d_u}{d_y} \quad (12)$$

Where d_α related to the displacement at αV_u . In this study the value of α is assumed 0.75 and 0.55 for no retrofitted and retrofitted models, respectively. It is necessary to mention the value $\alpha = 0.75$ was proposed for masonry structures (Magenes and Calvi 1997), but the value $\alpha = 0.55$

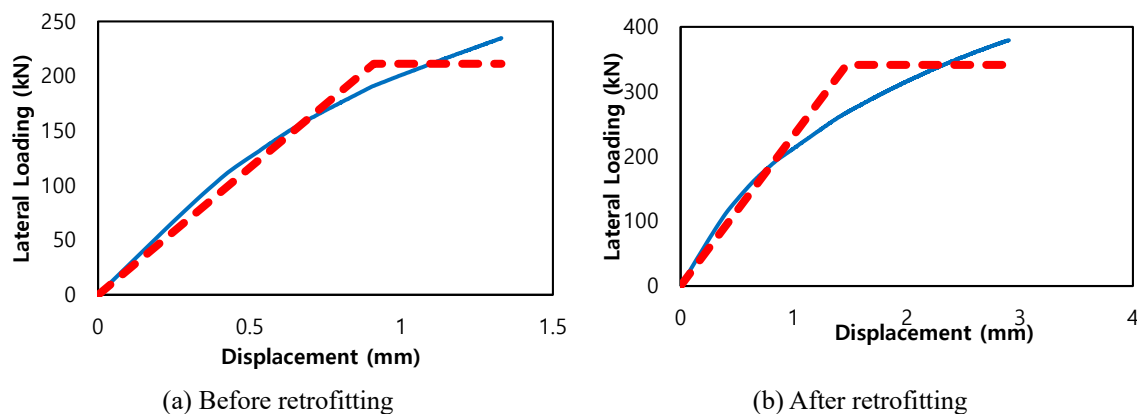


Fig. 14 Bilinear idealized curves of Prestwood bridge under seismic actions

is proposed in this study for retrofitted masonry structures based on this concept that the effective stiffness of bridge before and after retrofitting is similar to each other.

Moreover, energy dissipation (E_D) is defined as the area under backbone or bilinear idealized curves. Fig. 14 shows seismic capacity and bilinear idealized curves. The values of these parameters are determined and reported in Table 3. It is worth noticing that all parameters of bilinear idealized curves of retrofitted bridge are increased and the results indicate that the performance of retrofitted bridge by sprayed concrete technique improve the performance of masonry arch bridges under seismic actions.

5. Conclusions

There are almost 3500 masonry arch bridges within the railroad system of Iran. Gravity and vertical loads have only been considered for designing these structures, and earthquake loading has not been taken into account for the designing procedure. Hence, seismic evaluation appears to be essential for these structures. In Iran some of railway bridges have been retrofitted by sprayed concrete technique. So, in this study, firstly a masonry arch bridge was selected and using macro-modeling approach and the finite element analysis, the numerical model was validated. Then the in-plane cyclic behavior of a retrofitted masonry arch bridge evaluated. The results indicated that the performance of retrofitted bridge by sprayed concrete technique improve the total performance of masonry arch bridges under service and seismic actions. The increasing of seismic performance is far more than the vertical capacity. So, it can be concluded, in contrast to the 20% increase in service capacity of retrofitted models, the energy dissipation of retrofitted bridge increased about 300%. So, the sprayed concrete technique is recommended for seismic rehabilitation of single span masonry arch bridges and it is not proper for strengthening of masonry arch bridges under vertical live service loads.

References

Azimi, P. and Yazdani, M. (2022), "Calculation of dynamic amplification factor for railway concrete and

- masonry arch bridges subjected to high-speed trains (Article)", *Periodica Polytechnica Civil Engineering*, **66**(3), 876-890. <https://doi.org/10.3311/PPci.19494>.
- Chen, W.F. (2007), *Plasticity in reinforced concrete*. J. Ross Publishing.
- Committee, A. (2008), 'Building code requirements for structural concrete (ACI 318-08) and commentary'. American Concrete Institute.
- D'Ambrisi, A., Focacci, F. and Caporale, A. (2013), "Strengthening of masonry–unreinforced concrete railway bridges with PBO-FRCM materials", *Compos. Struct.*, **102**, 193-204. <https://doi.org/10.1016/j.compstruct.2013.03.002>.
- Drosopoulos, G.A., Stavroulakis, G.E. and Massalas, C.V. (2007), "FRP reinforcement of stone arch bridges: Unilateral contact models and limit analysis", *Compos. Part B: Eng.*, **38**(2), 144-151. <https://doi.org/10.1016/j.compositesb.2006.08.004>.
- Gönen, S. and Soyöz, S. (2021). "Seismic analysis of a masonry arch bridge using multiple methodologies", *Eng. Struct.*, **226**, 111354. <https://doi.org/10.1016/j.engstruct.2020.111354>.
- Gönen, S. and Soyöz, S. (2022), "Reliability-based seismic performance of masonry arch bridges", *Struct. Infrastruct. Eng.*, **18**(12), 1658-1673. <https://doi.org/10.1080/15732479.2021.1918726>.
- Homaei, F. and Yazdani, M. (2020), "The probabilistic seismic assessment of aged concrete arch bridges: The role of soil-structure interaction", *Structures*, **28**, 894-904. <https://doi.org/10.1016/j.istruc.2020.09.038>.
- Jahangiri, V., Yazdani, M. and Marefat, M.S. (2018), "Intensity measures for the seismic response assessment of plain concrete arch bridges", *Bull. Earthq. Eng.*, **16**(9), 4225-4248. <https://doi.org/10.1007/s10518-018-0334-8>.
- Magenes, G. and Calvi, G.M. (1997), "In-plane seismic response of brick masonry walls", *Earthq. Eng. Struct. D.*, **26**(11), 1091-1112. [https://doi.org/10.1002/\(SICI\)1096-9845\(199711\)26:11<1091::AID-EQE693>3.0.CO;2-6](https://doi.org/10.1002/(SICI)1096-9845(199711)26:11<1091::AID-EQE693>3.0.CO;2-6).
- Mahmoudi Moazam, A., Hasani, N. and Yazdani, M. (2017), "3D simulation of railway bridges for estimating fundamental frequency using geometrical and mechanical properties (Article)", *Adv. Comput. Design*, **2**(4), 257-271. <https://doi.org/10.12989/acd.2017.2.4.257>.
- Mahmoudi Moazam, A., Hasani, N. and Yazdani, M. (2018), "Three-dimensional modelling for seismic assessment of plain concrete arch bridges", *Proceedings of the Institution of Civil Engineers - Civil Engineering*, **171**(3), 135-143. <https://doi.org/10.1680/jcien.17.00048>.
- Marefat, M.S., Yazdani, M. and Jafari, M. (2019), "Seismic assessment of small to medium spans plain concrete arch bridges", *Eur. J. Environ. Civil Eng.*, **23**(7), 894-915. <https://doi.org/10.1080/19648189.2017.1320589>.
- Panian, R. and Yazdani, M. (2020), "Estimation of the service load capacity of plain concrete arch bridges using a novel approach: Stress intensity factor", *Structures*, **27**, 1521-1534. <https://doi.org/10.1016/j.istruc.2020.07.055>.
- Pantò, B., Grosman, S., Macorini, L. and Izzuddin, B.A. (2022), "A macro-modelling continuum approach with embedded discontinuities for the assessment of masonry arch bridges under earthquake loading", *Eng. Struct.*, **269**, 114722. <https://doi.org/10.1016/j.engstruct.2022.114722>.
- Sarhosis, V., De Santis, S. and de Felice, G. (2016), "A review of experimental investigations and assessment methods for masonry arch bridges", *Struct. Infrastruct. Eng.*, **12**(11), 1439-1464. [doi:10.1080/15732479.2015.1136655](https://doi.org/10.1080/15732479.2015.1136655).
- Sarhosis, V., Forgács, T. and Lemos, J.V. (2019), "A discrete approach for modelling backfill material in masonry arch bridges", *Comput. Struct.*, **224**, 106108. <https://doi.org/10.1016/j.compstruc.2019.106108>.
- Simoncello, N., Zampieri, P., Gonzalez-Libreros, J., Perboni, S. and Pellegrino, C. (2020), "Numerical analysis of an FRP-strengthened masonry arch bridge (Article)", *Front. Built Environ.*, **6**. <https://doi.org/10.3389/fbuil.2020.00007>.
- Wang, J. and Melbourne, C. (2010), "Mechanics of MEXE method for masonry arch bridge assessment", *Proceedings of the Institution of Civil Engineers - Engineering and Computational Mechanics*, **163**(3), 187-202. <https://doi.org/10.1680/eacm.2010.163.3.187>.
- Wang, Z., Yang, J., Zhou, J., Yan, K., Zhang, Z. and Zou, Y. (2022), "Strengthening of existing stone arch bridges using UHPC: Theoretical analysis and case study", *Structures*, **43**, 805-821.

- doi:<https://doi.org/10.1016/j.istruc.2022.06.055>.
- Yazdani, M. (2021), "Three-dimensional nonlinear finite element analysis for load-carrying capacity prediction of a railway arch bridge", *Int. J. Civil Eng.*, **19**(7), 823-836. <https://doi.org/10.1007/s40999-021-00608-w>.
- Yazdani, M. and Habibi, H. (2023), "Residual capacity evaluation of masonry arch bridges by extended finite element method", *Struct. Eng. Int.*, **33**(1), 183-194. <https://doi.org/10.1080/10168664.2021.1944454>.
- Yazdani, M. and Jahangiri, V. (2020), "Intensity measure-based probabilistic seismic evaluation and vulnerability assessment of ageing bridges (Article)", *Earthq. Struct.*, **19**(5), 379-393. <https://doi.org/10.12989/eas.2020.19.5.379>.
- Zampieri, P., Zanini, M.A. and Modena, C. (2015), "Simplified seismic assessment of multi-span masonry arch bridges", *Bull. Earthq. Eng.*, **13**(9), 2629-2646. <https://doi.org/10.1007/s10518-015-9733-2>.